Supplementary Information: Stress drop heterogeneity within tectonically complex regions: A case study of San Gorgonio Pass, southern California

T. H. W. Goebel[1], E. Hauksson[1], P. M. Shearer[2], and J. P. Ampuero[1]

[1]Caltech Seismological Laboratory, Pasadena, California, USA.
[2]Scripps Institution of Oceanography, University of California, San Diego, California, USA.

1 Method

The recorded seismic waveforms are a convolution of site, path and source contributions. Our source spectral inversion makes use of common ray-paths and site-effects for event clusters recorded at the same station, and common source terms for events recorded over an array of near-by stations (Figure 1). Source spectra are obtained by iteratively stacking the recorded amplitude spectra to isolate source, path and site terms (e.g. *Andrews*, 1986; *Warren and Shearer*, 2000; *Shearer et al.*, 2006; *Yang et al.*, 2009). The parameter choices and frequency bands used for the spectral stacking and stress drop estimates can be found in Table 1.

Description	Parameter value or frequency range
P-wave time window	1.28 s
minimum signal to noise ratio	5 (varied between 3 to 10)
minimum number of seismic records	5 (varied between 5 to 15)
Range of low frequencies for Ω_0 computations	first 3 sample points >1 Hz (1.6–3.1 Hz)
Frequency band for SNR computations	5–10, 10–15, 15–20 Hz
Frequency band for amplitude spectra	0.2–50 Hz
Frequency band for fitting Brune-type spectral models	2–20 Hz

Table 1: Parameter choices and frequency bands used to compute spectra, corner frequencies and stress drops.

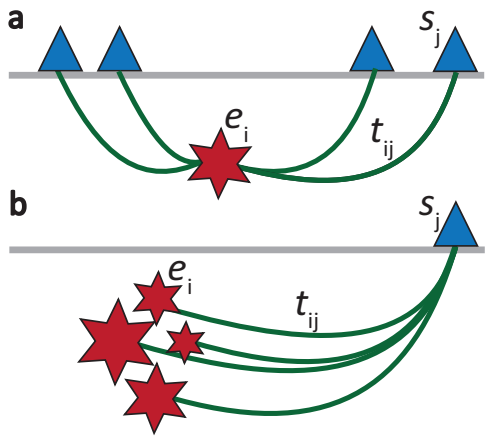

Figure 1: Schematic image of ray-paths of event waveforms recorded at different stations (a), and different events within a small region recorded at the same station (b). The recorded waveforms are a convolution of source (e_i), path (t_{ij}) and site (s_j) contributions.

1.1 Stacked source and path terms and determination of empirical Green's function

After inverting the recorded spectra for average source terms of individual earthquakes, we stacked the event spectra within common magnitude bins resulting in relatively smooth, average spectra (Figure 2a). The smoothness of these spectra is a function of the number of recorded events within each magnitude bin, so that the relatively largest and lowest magnitude bins show the strongest spectral fluctuations. Consequently, we limit the following analysis to magnitude bins with 5 or more recordings. We observed the expected characteristics for a displacement spectra of a simple circular, symmetric rupture, i.e., approximately constant low-frequency amplitudes, a corner frequency that increases with decreasing relative moment and a high-frequency fall-off rate with an exponent of f^{-2}. Consequently, the stacked spectra can be described by a Brune-type spectral model after correcting high-frequency attenuation using a regional empirical Green's function. Moreover, the corner frequency and seismic moments are approximately proportional which is best seen after log-transformation and shifting the source spectra along the line of proportionality, thus effectively correcting for differences in moments between the events (Figure 2b). After this correction, the spectra largely collapse onto the same curve thus highlighting self-similar source parameter scaling at a regional scale.

Although the stacked source spectra for the entire study region show constant stress drops and self-similar source scaling, we observed strong spatial variations of stress drops within the study

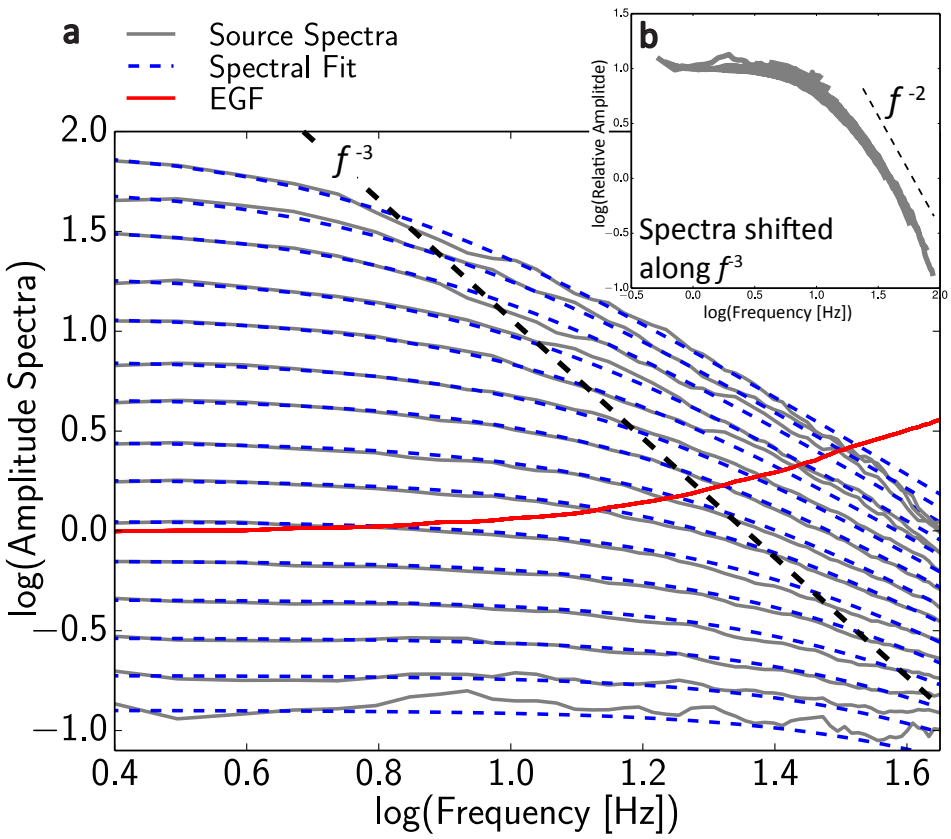

Figure 2: Source spectra stacked over events within 0.2 magnitude bins (gray curves) and corresponding Brune-type spectral fits (blue dashed lines). The red curve represents the regional average empirical Green's function used to correct high frequency contributions and the black dashed line highlights the line of constant stress drop for which $M_0 \propto f_c^{-3}$. This relationship is also used to correct for differences in moments by shifting along f^{-3} until the low frequency moments coincide (b).

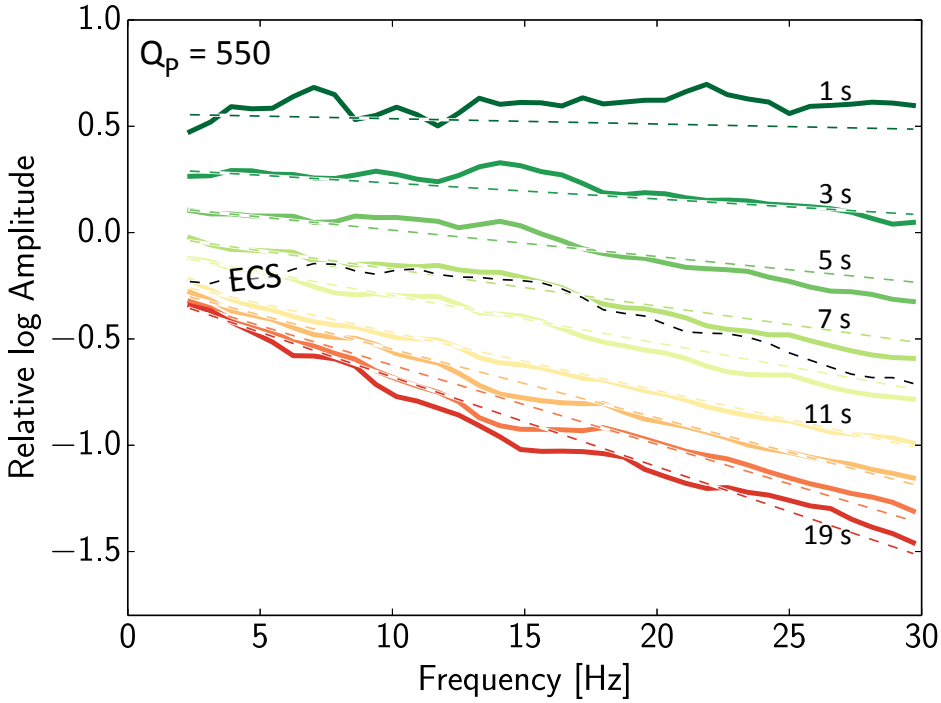

Figure 3: Average path terms (solid lines) stacked within 2 s bins and empirical correction function (ECS). The ECS is computed by averaging the misfit between an exponential attenuation model with Q_P=550 (curves, colored with travel-time), analogous to *Shearer et al.* (2006). The ECS removes the ambiguity with respect to a constant log spectrum that could be added and subtracted from any pair of terms in Equation 1 in the main manuscript, similar to the EGF used to correct the source spectra.

region. This variation can, for example, be observed for individual event spectra with similar relative moments. For a self-similar rupture, these spectra should show approximately constant corner frequencies. Our results, on the other hand, highlight strong variations in corner frequencies and stress drops (Figure 4).

2 Sensitivity analysis of stress drop computations

We tested for systematic biases of the spectral fits as function of stress drop, for example, due to poor fits of events within a specific stress drop range. The root-mean-square misfits between modeled and observed spectra showed little variations within the core range of stress drop, i.e. between $\sim$1 and $\sim$40 MPa (Figure 5), highlighting that even high stress drop estimates stem from spectral fits with relatively small misfits.

Furthermore, we ensured a sufficient azimuthal coverage and waveform quality, by requiring events to be recorded at $\geq$5 stations (N_{spec}) with a signal-to-noise ratio (SNR) of ≥ 5. Based on these quality criteria, we computed stress drops of individual seismic events which follow a log-normal distribution with a mean value of $\Delta\sigma \sim 4.8$ MPa. We also tested the influence of input parameter choices revealing relatively stable mean values even though the distribution-tails may vary substantially (Figure 6).

To further test the robustness of spatial variations in stress drop, we performed source spectral inversions for events within the low and high stress drop region while varying the parameters SNR, and N_{spec}. As expected, higher constrains on spectral quality, i.e. higher values for SNR and N_{spec} reduced the total amount of spectra by a factor of 2–8 which primarily led to a decrease in stress drop scatter within the lower moment ranges (Figure 7). The corresponding mean stress drops changed by a factor of 1.2–2, however, these variations in mean values did not significantly alter the difference between low and high stress drop regions, leading to a slight enhancement of the difference in stress drops.

We conducted a systematic test of the influence of the input parameters of the spectra inversions for two sub-regions with different stress drop (Figure 8). Increasing the minimum amount of required spectra, N_{spec}, decreased the misfit between spectral models and observations, i.e., the spectra conform more closely to a Brune-type model. For more restrictive quality criteria of the spectra, there was also a slight increase in the uncertainty of mean stress drops caused by fewer

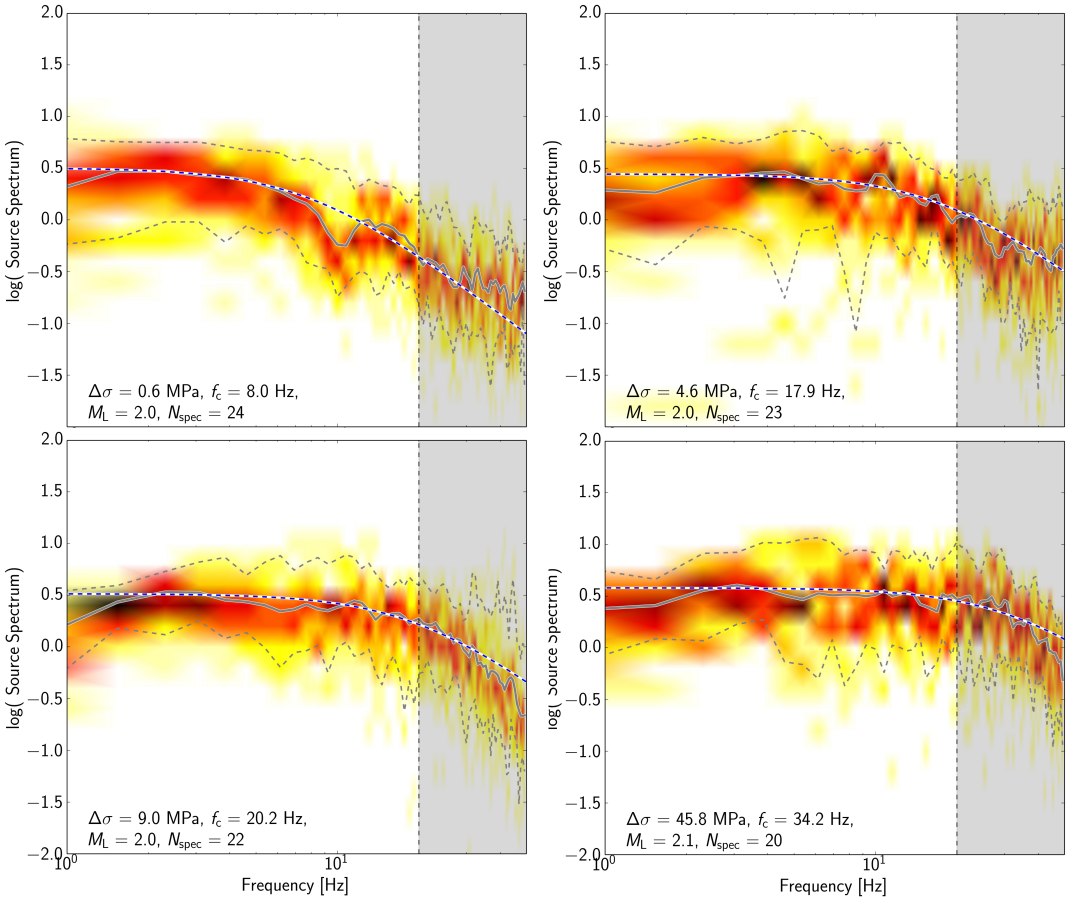

Figure 4: Example of four events with strongly varying stress drops, i.e., similar relative moments (low frequency content) but different corner frequencies. The gray curve highlights the average source spectra for all stations and the colored areas in the background show the density of spectra from individual stations, so that warmer colors correspond to higher density of spectra. The blue dashed lines show the Brune-type spectral fits and gray, dashed curves represent the confidence bounds of the spectral density estimates as a function of frequency. The gray, shaded frequency range above 20 Hz was not included during the computation of the spectral fits.

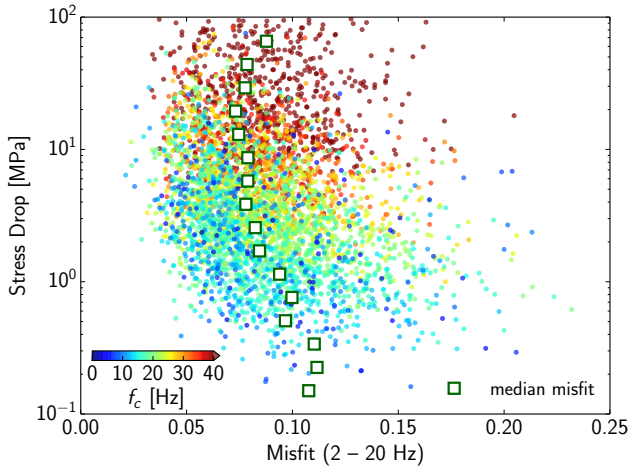

Figure 5: Changes in root-mean-square misfit between observed and modeled source spectra for different stress drop values. The round markers are colored according to corner frequency. The square markers show the average *rms*-values for different stress drop magnitudes.

events within the corresponding distributions. The high stress drop region shows a strong sensitivity to an increase in N_{spec} which was not observed for the tests on the whole data set (see Figure 6). This systematic change maybe due to the strong restrictions on the quality of the seismic record resulting in a small set of computed source spectra. The total number of spectra between $N_{\text{spec}} \geq 5$ and $N_{\text{spec}} \geq 15$ is reduced from ∼450 to ∼50.

If we perform a similar analysis on a larger data set, the mean stress drops are largely independent of N_{spec} (Figure 9a). The high and low stress drop regions still vary by a factor of 4, however, the absolute values are smaller most likely due to averaging over a larger region and including more events with relatively low stress drops. The stress drops for both high and low stress drop regions decrease with increasing SNR while the relative difference between the two regions remains constant (Figure 9b). Thus, we conclude that the absolute stress drop values are somewhat sensitive to the particular parameter choices and the selection criteria of the spectra that are the basis of source spectra inversions and stress drop estimates. This sensitivity becomes especially pronounced for small data sets. However, the relative differences between low and high stress drop regions are robust if the data are analyzed consistently.

We examined if the observed spatial variations in stress drops, including the high stress drop region between the traces of San Gorgonio thrust and Mission creek faults, are sensitive to changes in SNR and N_{spec}. The corresponding stress drop map (Figure 10) highlights similar lateral vari-

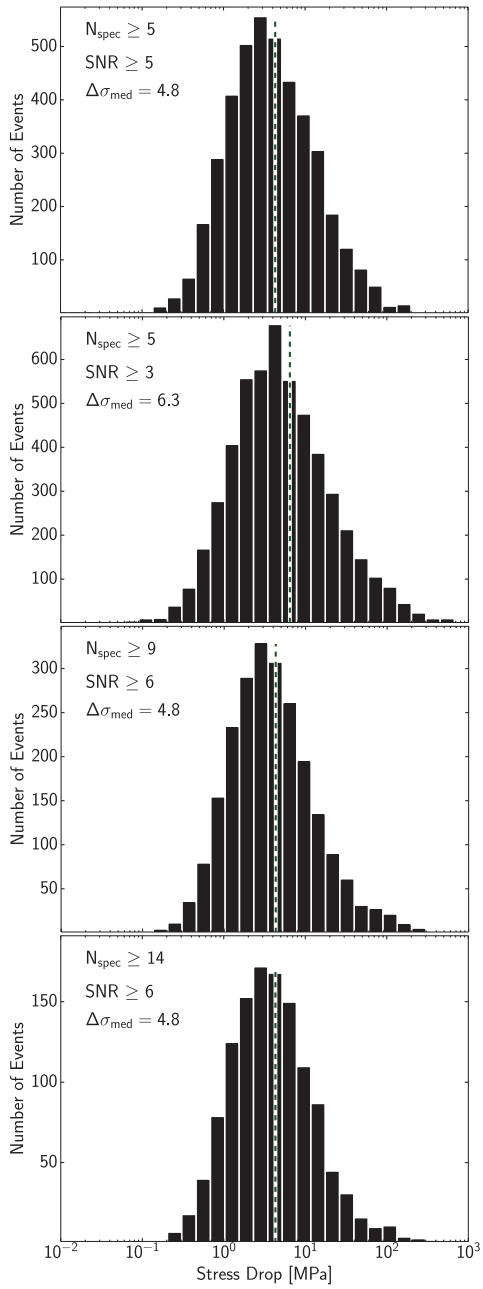

Figure 6: Histograms of stress drop values for different input parameters, SNR, and N_{spec} of the source inversions. The parameters are displayed in the upper left of each subplot together with the mean stress drops which showed only small variations. The top frame depicts the input parameters used for the analysis in the main manuscript.

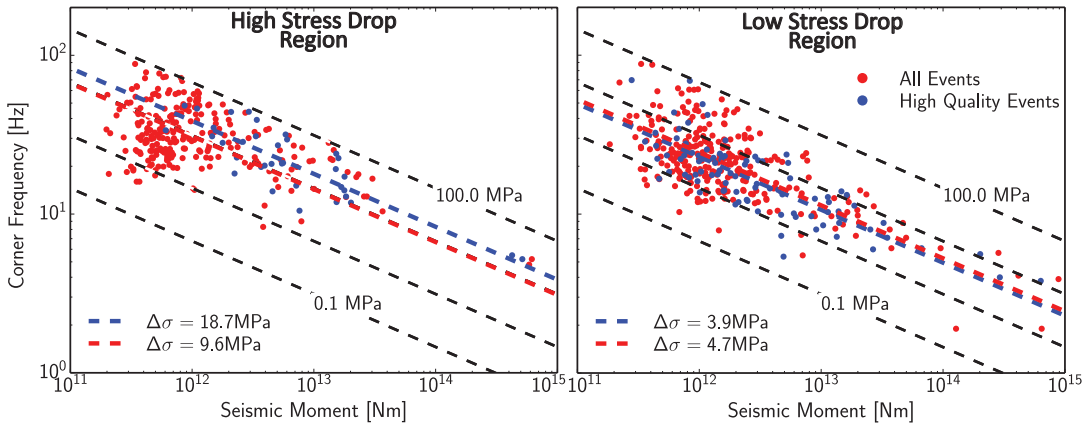

Figure 7: Corner frequency as a function of seismic moment for a less (red markers) and a highly (blue markers) restrictive selection of spectral quality criteria. The latter results in an exclusion of many small magnitude events from the analysis but also reduces the scatter substantially, especially, for spectra with small seismic moments. The corresponding mean stress drops (red and blue, dashed lines) change by a factor of ∼1.2–2 while preserving the difference between low and high stress drop regions.

ations (see also Figure 3 in the main manuscript), thus further supporting the robustness of the described stress drop variations.

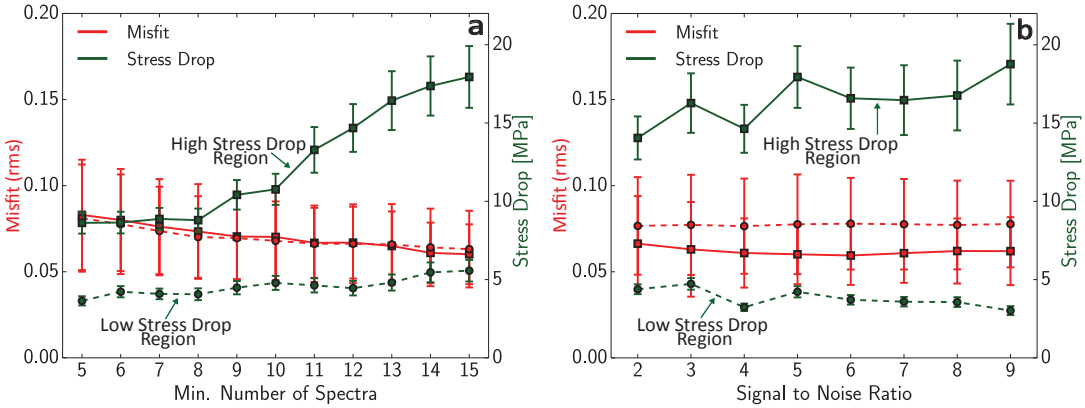

Figure 8: Variations in stress drops (green) and misfit (red) between source spectra and Brune-type model as function of N_{spec} (a) and SNR (b). The dashed lines depict results for a low stress drop region and solid lines for a high stress drop region.

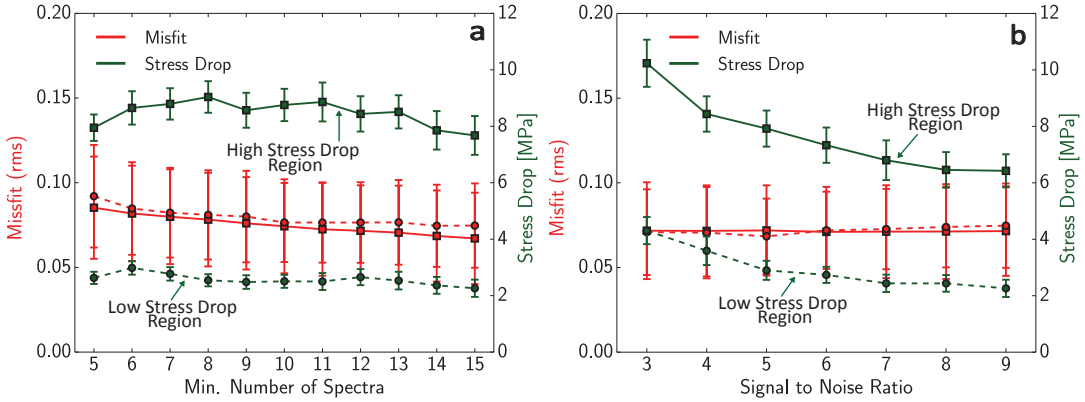

Figure 9: Same as Figure 8 but now for a larger region. The absolute stress drops decrease due to smoothing over larger areas, however, the difference between low and high stress drop region remains.

3 Influence of high-quality spectra on stress drop variations

In the following, we show changes in stress drops as a function of depth, focal mechanism type and geologic slip rate for more restrictive initial data selection criteria. These selection criteria are the minimum number of stations that recorded an event and the signal-to-noise ratio over three different bandwidth. The criteria quantify the overall quality of the seismic record for each event. A comparison between the variations in stress drops with depth (Figure 11), focal mechanism (Figure 12) and slip rates (Figure 13) between the complete and high-quality datasets (i.e. $N_{\text{spec}} = 15$, SNR=10) yields largely the same variations as described in the main manuscript. The following three figures are the same as Figures 7, 9 and 10 in the main manuscript with added results for high

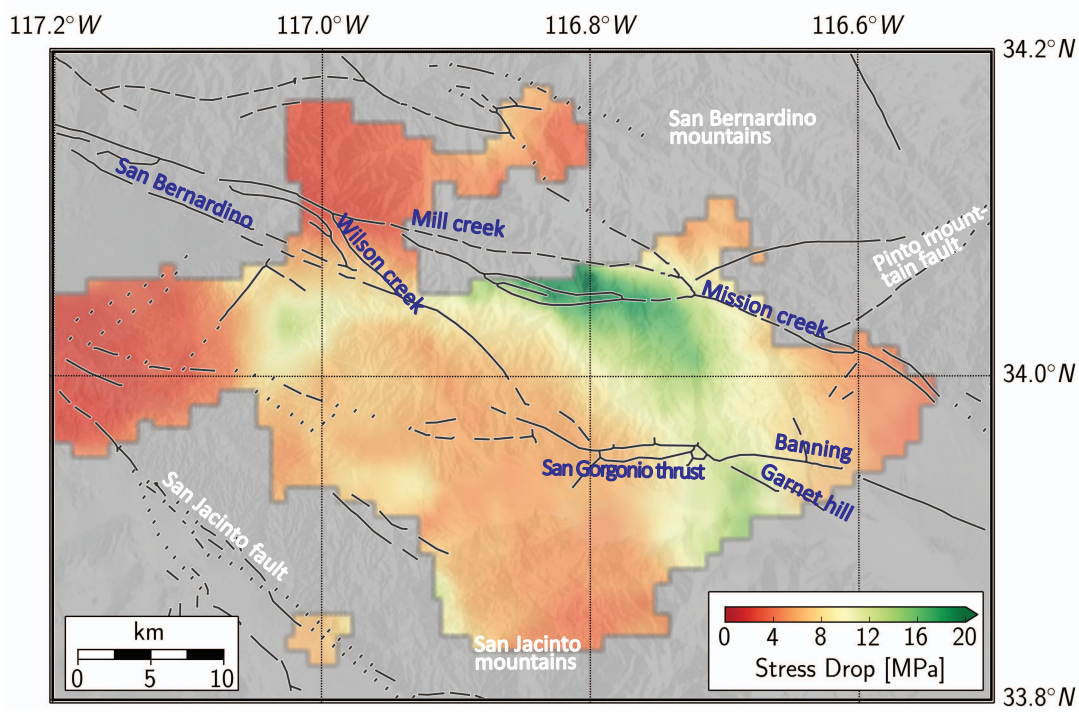

Figure 10: Smoothed spatial variations of stress drops computed from spectra with SNR≥6 and $N_{\text{spec}} \geq 12$. The overall pattern of low and high stress drop regions is similar to that in Figure 3 of the main manuscript.

quality datasets.

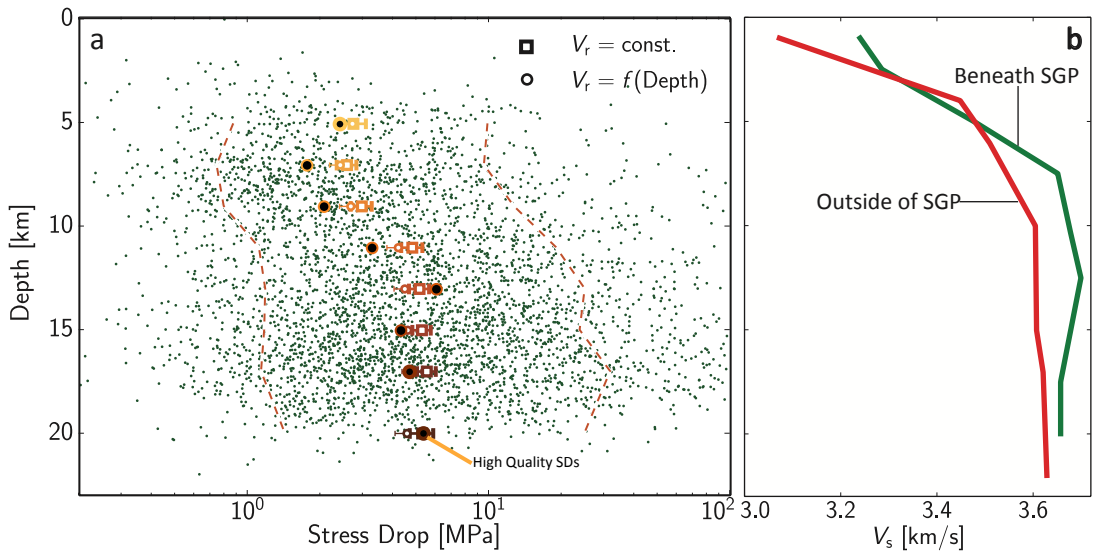

Figure 11: Variations in stress drops as a function of depth. The figure is the same as Figure 7 in the main manuscript with added stress drop results for the high quality dataset (black dots).

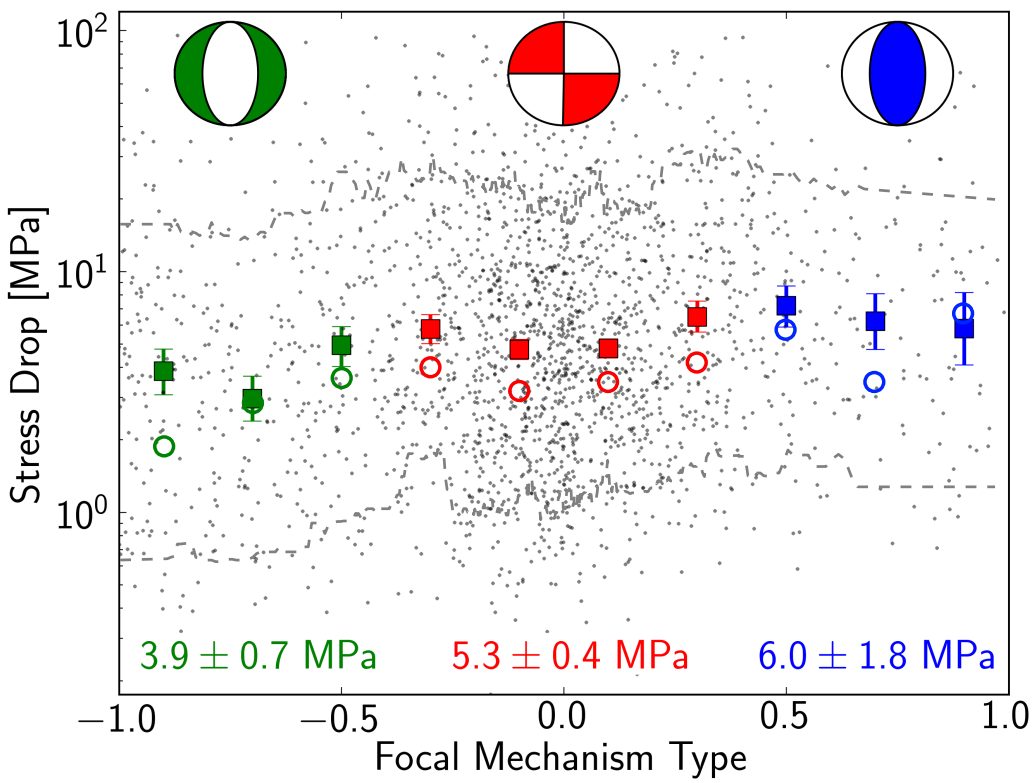

Figure 12: Variations in stress drops as a function of focal mechanism type. The figure is the same as Figure 9 in the main manuscript with added stress drop results for the high quality dataset (open circles).

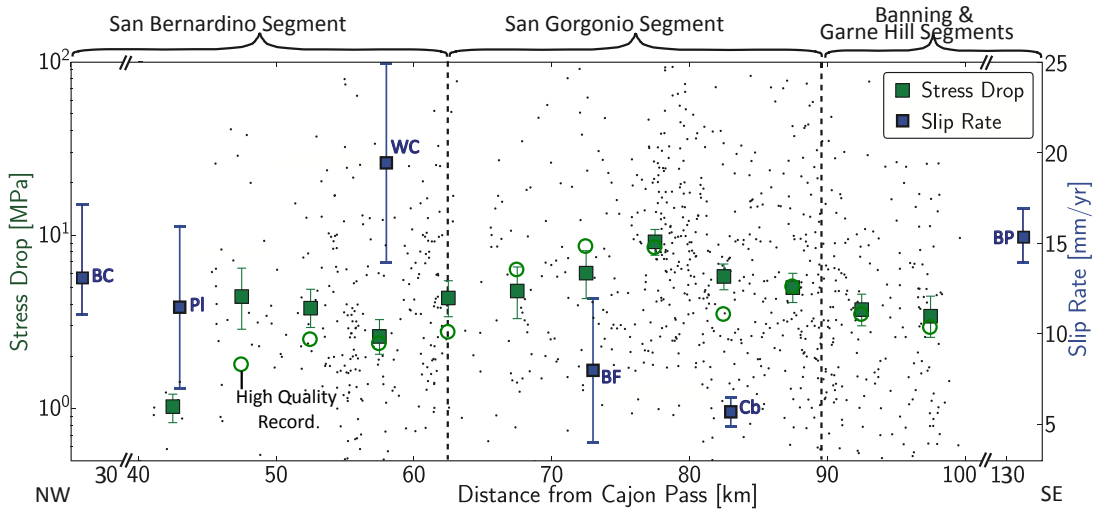

Figure 13: Variations in stress drops as a function of geological slip rates. The figure is the same as Figure 10 in the main manuscript with added stress drop results for the high quality dataset (open circles).

4 Statistical significance of stress-drop variations

We tested if the observed, systematic variations in stress drops are statistically significant. To this aim, we used three different significance tests: 1) the non-parametric Kolmogorov-Smirnoff test (KS-test); 2) the student's t-test using the log-transformed data; and 3) we resampled the medians of two observed distributions 1000 times to quantify the expected statistical variation. Both test 1) and 3) are not dependent on assumptions on underlying distributions. Test 2) and 3) are largely insensitive to differences in the distribution's scale so that distributions with different scales but similar mean-values would still fail these tests. The KS-test is thus a more stringent test for similarity between two distributions. Nonetheless, we chose a conservative approach, rejecting the null-hypothesis $H_0 : \mu_1 = \mu_2$ only if $p \leq 0.01$, where μ_1 and μ_2 are the parameters (i.e. median or log-normal mean) of the two different distributions.

Our tests revealed that depending on the absolute values and the number of events within a population, variations of 1–2 MPa can be statistically significant. Except for stress drop variations as function of focal-mechanism type, the observed stress drop variations can be considered as statistically significant at a 99% level.

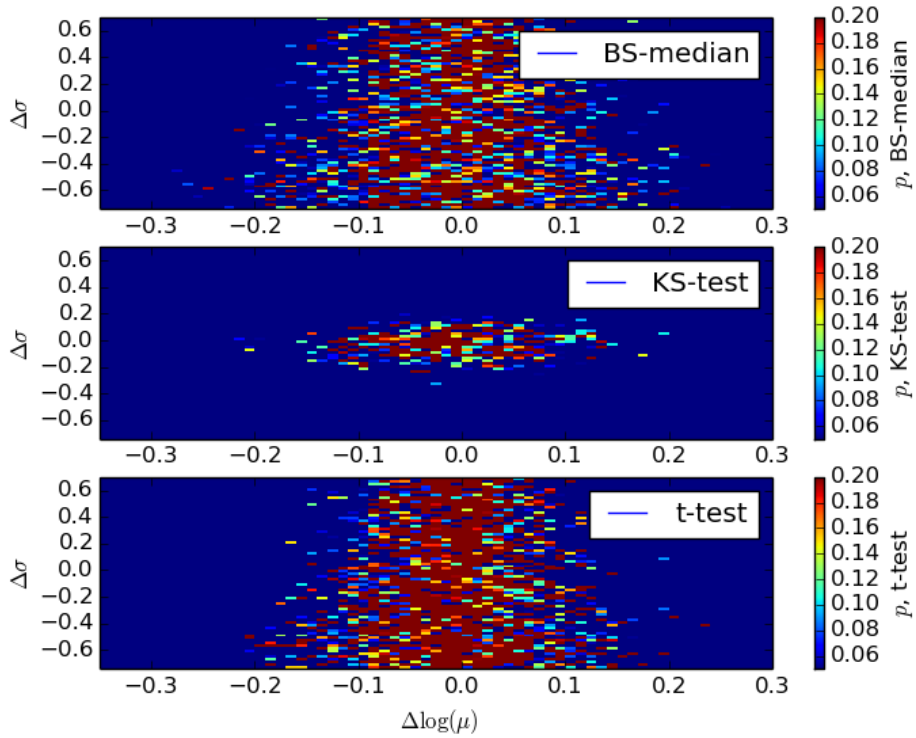

Figure 14: Comparison between different parametric and non-parametric tests to determine if variations in stress-drop distributions are statistically significant (see text for details). The shown results are for synthetic log-normal distributions with mean values between 1–10 MPa. $\Delta\sigma$ is the corresponding parameter that controls the changes in scale and $\Delta\log(\mu)$ specifies the difference in mean of the log-transformed data (here log refers to the natural logarithm).

References

Andrews, D. J. (1986), Objective determination of source parameters and similarity of earthquakes of different size, *in Earthquake Source Mechanics*, pp. 259–267, doi:10.1029/GM037p0259.

Shearer, P. M., G. A. Prieto, and E. Hauksson (2006), Comprehensive analysis of earthquake source spectra in southern California, *J. Geophs. Res.*, *111*(B6), B06,303.

Warren, L. M., and P. M. Shearer (2000), Investigating the frequency dependence of mantle Q by stacking P and PP spectra, *J. Geophys. Res.*, *105*(B11), 25,391–25.

Yang, W., Z. Peng, and Y. Ben-Zion (2009), Variations of strain-drops of aftershocks of the 1999

Population types	diff. $\Delta\sigma$ [MPa]	p_{med}	p_{KS}	p_{t}
low/high $\Delta\sigma$ region	4.9–17.3	<0.01	<0.01	<0.01
normal/strike-slip foc. mech.	1.4	0.01	<0.01	<0.01
strike-slip/thrust foc. mech.	0.7	0.29	0.14	0.16
7/15 km depth	2.7	<0.01	<0.01	<0.01
56/78 km distance from Cajon pass	6.9	<0.01	<0.01	<0.01

Table 2: Difference in stress-drop estimates (diff. $\Delta\sigma$) and statistical significance for a non-parametric test and tests assuming log-normally distributed data. Population types refer to the two different populations that are compared: low/high $\Delta\sigma$ region: A low and high stress-drop region (see Figure 3b in main manuscript); normal/strike-slip foc. mech.: predominantly normal vs. strike-slip focal mechanisms; and strike-slip/thrust foc. mech.: strike-slip vs. thrust focal mechanisms; 7/15 km depth: Stress drop estimates at 7 and 15 km depth; 56/78 km distance from Cajon pass: Stress-drop estimates along the San Andreas fault zone at 56 and 78 km distance from Cajon Pass.

İzmit and Düzce earthquakes around the Karadere-Düzce branch of the North Anatolian Fault, *Geophys. J. Int.*, *177*(1), 235–246.